Unfolding in ATLAS

Georgios Choudalakis
University of Chicago, on behalf of the ATLAS Collaboration

Abstract
This article presents the unfolding techniques used so far in ATLAS. Two representative examples are discussed in detail; one using bin-by-bin correction factors, and the other iterative unfolding.

1 Introduction

The distribution of any observable is distorted due to experimental limitations. Unfolding is the procedure of estimating the "truth-level" spectrum, i.e., the spectrum that would be measured with an ideal detector and infinite event statistics. A general introduction to unfolding, and details about various methods are given in other contributions to this workshop. The focus here will be on real life examples of unfolding in ATLAS analyses.

As of early 2011, ATLAS has used two unfolding methods:

 i) bin-by-bin correction factors;
ii) the iterative method by D'Agostini [1].

One representative example will be presented from each method. In Section 2, bin-by-bin correction is presented through the inclusive jet p_T spectrum measurement [2]. In Section 3, D' Agostini's iterative method [1] is presented, as it was used to estimate the spectrum of charged particle multiplicity in minimum bias interactions [3].

Both methods have drawbacks. An insightful overview can be found in [4], and in other contributions to this workshop. Bin-by-bin correction has been particularly criticized for not dealing carefully with bin correlations, among other things. ATLAS is considering methods beyond bin-by-bin in the next round of analyses where this method was used.

In searches for new physics, ATLAS does not apply any unfolding, because it is unnecessary for making a discovery, or for setting a limit to some model, or for estimating model parameters. Unfolding can be regarded as useful when the distribution itself (or a binned version thereof) is regarded as the set of parameters of interest.
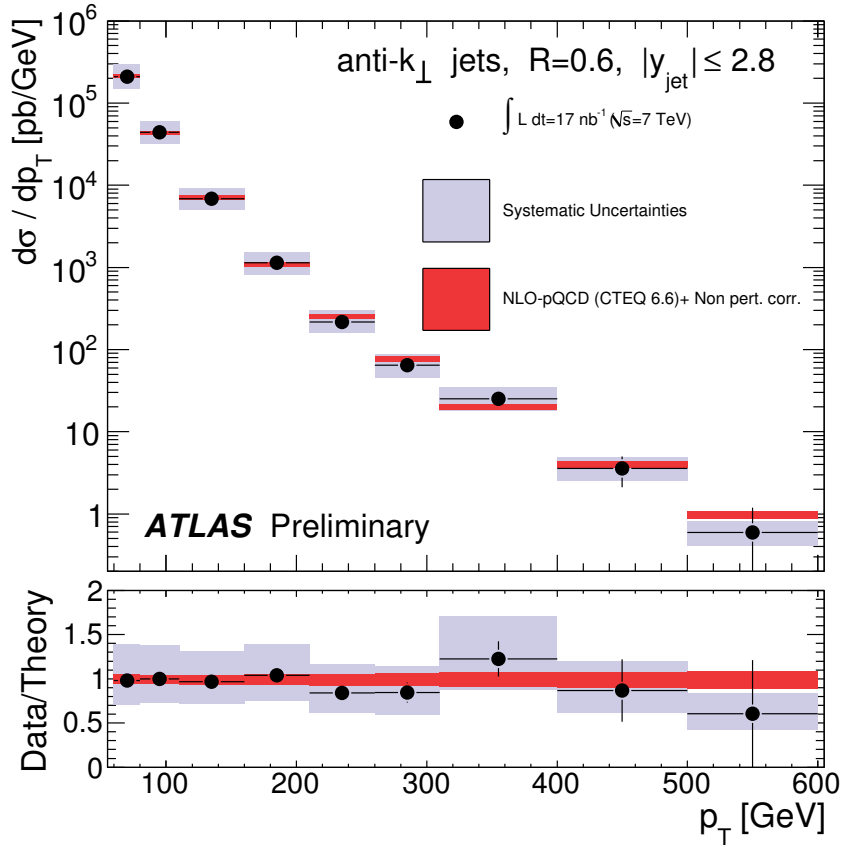
2 Bin-by-bin correction factors

Several ATLAS analyses have used the method of bin-by-bin correction factors [2,5–7], mostly because of its simplicity. The example of inclusive jet p_T measurement [2] will be discussed. The main result of this measurement is shown in Fig. 1. In this analysis truth-level corresponds to hadron-level.

2.1 Method description

Let T_i be the expected number of events in bin i of the truth-level p_T spectrum, which is obtained from Monte Carlo (MC). Leading order PYTHIA [8] QCD MC was used in the case of [2], where no event selection was applied. The truth-level p_T spectrum contains jets reconstructed after hadronization, applying the anti-k_T clustering algorithm on stable hadrons produced after fragmentation and hadronization. Detector simulation is not involved in the truth-level spectrum.

Let R_i be the expected number of events in bin i of the measured p_T spectrum, which suffers from detector smearing, after event selection which includes trigger requirements, jet reconstruction

Fig. 1: The estimated truth-level spectrum of inclusive jet p_T (filled markers) from [2], obtained using bin-by-bin correction factors, compared to the theoretical truth-level QCD prediction (red band). The black error bars represent the statistical uncertainty of the estimated spectrum, and the blue band the total systematic uncertainty, which is obtained by summing in quadrature individual systematic uncertainties. The dominant contribution comes from the jet energy scale uncertainty. In each bin the estimated truth-level spectrum has been divided by the width of the bin and by the integrated luminosity, whose uncertainty (11%) is not included in the blue error band.

inefficiency at low p_T, primary vertex requirements, jet quality criteria etc. The same PYTHIA QCD MC is used as before, after ATLAS detector simulation, to obtain R_i. Jets are reconstructed by applying the same anti-k_T algorithm on topological clusters of energy deposited in the calorimeter [9].

Let D_i be the actually observed number of events in bin i of the measured p_T spectrum. Whereas T_i and R_i are both real numbers after normalizing the MC samples to the integrated luminosity of the available dataset, D_i can only take integer values, because the observed events are discrete. If it is assumed that R_i is the result of an ideal simulation of all physical processes that occur at the proton collisions[1] and of the ATLAS detector, then D_i is a random integer that follows a Poisson distribution with mean R_i.

$$C_i \equiv \frac{T_i}{R_i}, \tag{1}$$

be the correction factor corresponding to bin i of the observed p_T spectrum. The correction factors used in [2] are shown in Fig. 2.

---

[1]Obviously this is not a good assumption when one acknowledges the possibility of new physics, but in measurements such as the one we discuss here it is presumed that what is measured is just QCD.
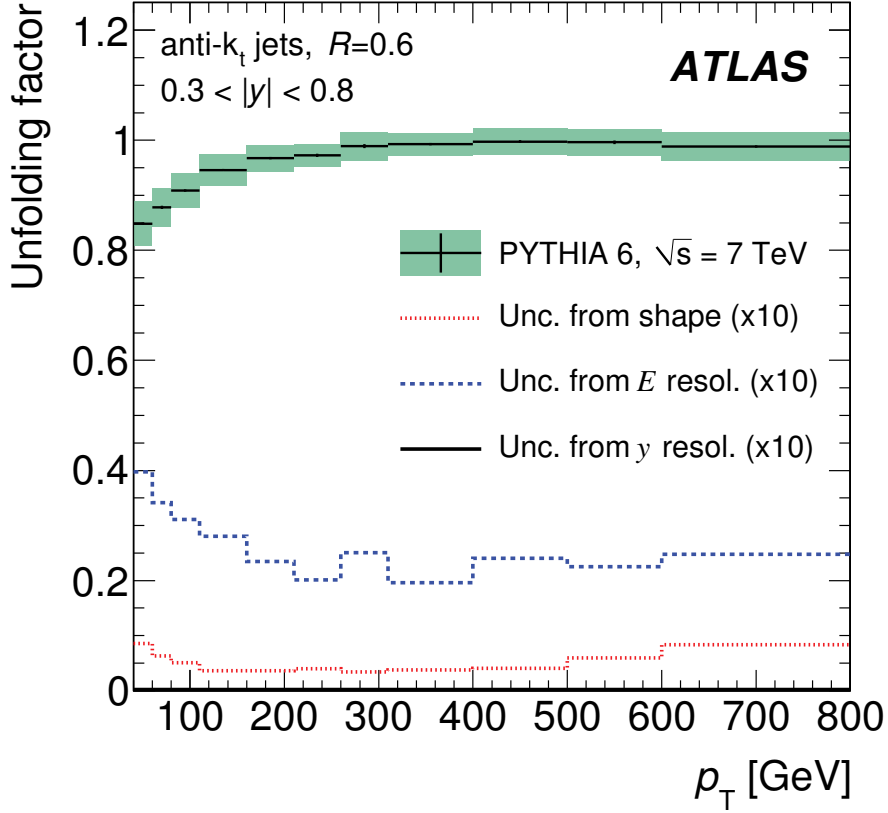
Fig. 2: The correction factors (C_i) used in [2]. The statistical uncertainties (black crosses) are invisibly small. The green band represents the total systematic uncertainty, except for the part which is due to jet energy scale, which is discussed in Section 2.3.4.

The answer returned for bin i of the truth-level p_T spectrum after bin-by-bin correction is

$$U_i \equiv C_i \cdot D_i. \tag{2}$$

U_i is the estimator of T_i.

2.1.1 Bias

The estimator U_i has a bias that is easy to compute.

Let's consider the possibility that the truth-level spectrum is actually T_i', which may differ from the assumed T_i. This could happen, for example, if sizable processes other than those included in PYTHIA QCD are occurring in nature, or if the modeling of QCD by PYTHIA is unrealistic. Let's also assume that the actual expected spectrum at detector level is R_i', which may differ from R_i for the above reasons, as well as due to unrealistic modeling of the detector response and of the quantities involved in event selection. The bias of the estimator U_i then is

$$\langle U_i - T_i' \rangle = \langle \frac{T_i}{R_i} D_i - T_i' \rangle = \frac{T_i}{R_i} \langle D_i \rangle - T_i' = \frac{T_i}{R_i} R_i' - T_i' = \left(\frac{T_i}{R_i} - \frac{T_i'}{R_i'} \right) R_i'. \tag{3}$$
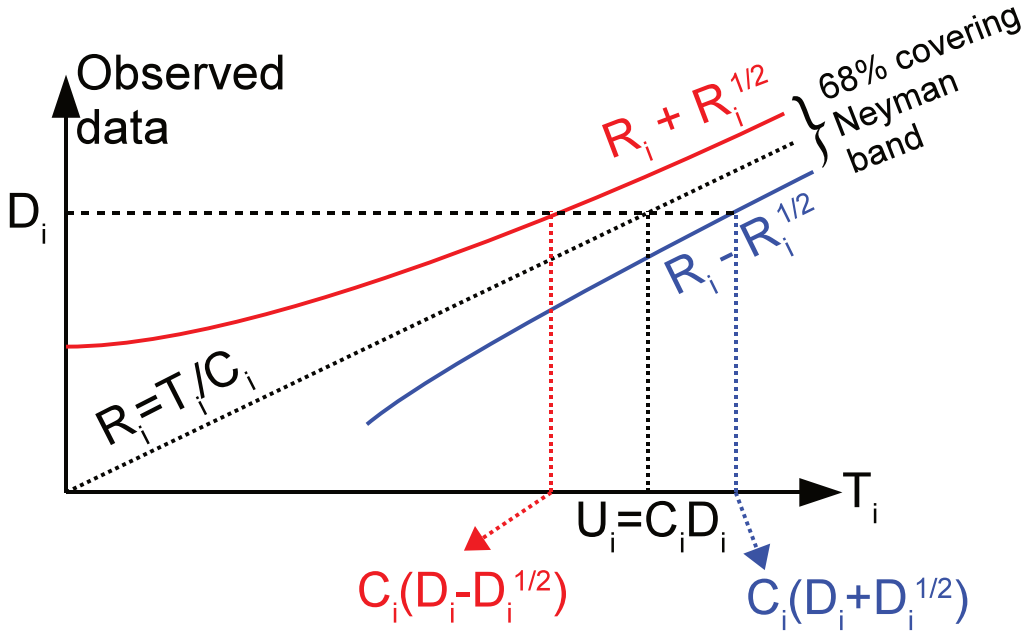
Fig. 3: Sketch of the Neyman construction used to correspond an observed number of data events D_i to a 68% confidence interval for T_i in the bin-by-bin correction factor method. The definitions of D_i, T_i, R_i, C_i and U_i are given in Sec. 2.1. For large values of T, the upper and lower bounds of the Neyman band follow asymptotically $R_i + \sqrt{R_i}$ and $R_i - \sqrt{R_i}$ respectively. At low values of T, where Poisson is not well-approximated by a Gaussian, the Neyman band is not symmetric around R_i, which is the reason that in this sketch the bounds of the Neyman band are obscured at low T.

2.2 Statistical uncertainty

The Neyman construction shown in Fig. 3 is effectively used to obtain a confidence interval for T_i, given C_i and the data D_i. Having observed D_i, the 68% confidence interval (CI) for U_i is approximately

$$C_i(D_i \pm \sqrt{D_i}). \tag{4}$$

This is a fair approximation when D_i is large, in which case the Poisson distribution of D_i with mean R_i is similar to a Gaussian of mean R_i and standard deviation $\sqrt{R_i}$. Although this approximation fails in bins with few data, the same formula was used in all p_T bins, so for all bins it was assumed that the statistical uncertainty of U_i is symmetric and equal to

$$\sigma_{U_i} = C_i\sqrt{D_i}. \tag{5}$$

This is the size of the black error bars in Fig. 1.

2.3 Systematic uncertainty

The following main sources of systematic uncertainty were identified in [2]:

i) the correction factor C_i is subject to statistical fluctuations due to finite MC event statistics;

ii) the amount of p_T smearing in detector simulation may be unrealistic;

iii) the used spectrum of T_i may be unrealistic;

iv) jet energy scale uncertainty.

The following paragraphs describe how each systematic uncertainty was propagated to the final estimator of the truth-level spectrum.
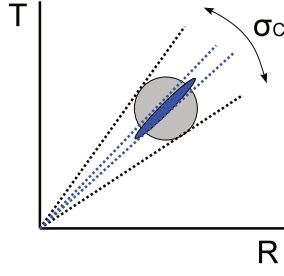
Fig. 4: The effect of covariance between T_i and R_i in the variance of the correction factor C_i. The gray circle indicates the case of zero covariance, and the dark ellipse the case of highly positive correlation.

2.3.1 Finite MC event statistics

The correction factors C_i have some uncertainty due to random fluctuations of the finite MC event statistics available to determine T_i and R_i. When T_i fluctuates above its mean, so does R_i, so the two are highly correlated (Fig. 4). The statistical uncertainty in C_i was computed taking this correlation into account, as follows:

The MC events which compose R_i ($N(R_i)$) are separated into those coming from the same truth-level bin ($N(R_i \wedge T_i)$) and those coming from different truth-level bins ($N(R_i \wedge \neg T_i)$).[2] Similarly, the $N(T_i)$ MC events which contribute to T_i are separated into those that end up in the same bin after detector simulation and event selection ($N(T_i \wedge R_i)$), and those that migrate to different bins ($N(T_i \wedge \neg R_i)$). The variables $N(T_i \wedge R_i)$ and $N(R_i \wedge T_i)$ are identical. So, C_i can be expressed as a function of three statistically independent random variables:

$$C_i = \frac{T_i}{R_i} = \frac{N(T_i \wedge R_i) + N(T_i \wedge \neg R_i)}{N(T_i \wedge R_i) + N(R_i \wedge \neg T_i)}. \tag{6}$$

Since C_i is expressed as a function of three statistically uncorrelated variables, error propagation can be used where covariance terms are zero. Each one of the three MC event populations has standard deviation $\sqrt{N}$.

2.3.2 Jet p_T resolution uncertainty

A relative systematic uncertainty of 15% in jet p_T resolution was assumed, based on the results of in-situ studies [10].

To model the effect of a different p_T resolution on C_i, the jets in MC events were smeared by an additional amount α, which varied from 0 to 20% of the nominal smearing that is present in ATLAS MC. For each amount of extra smearing, the values of R_i change, while T_i is not affected. As a result each correction factor C_i has a dependence on the amount of extra smearing. It was furthermore observed that in all bins i the correction factor C_i varied linearly with α.

It is possible to increase the smearing of jet p_T by adding to it a random offset of appropriate variance, but it is not possible to do the opposite, i.e., to reduce the amount of smearing that is nominally present in the ATLAS MC. This complicates the task of determining the uncertainty on C_i, because the resolution uncertainty of 15% is symmetric; the jet p_T resolution could be 15% worse or 15% better than its nominal value. The observation that C_i depends linearly on the extra smearing justifies the assumption that, if the resolution improved, C_i would still vary linearly.

---

[2]The symbol $\wedge$ is the logical "and", while $\neg$ is the logical "not". So, $R_i \wedge \neg T_i$ means belonging in R_i *and not* in T_i.

2.3.3 Uncertainty in spectrum shape

The correction factors C_i depend on the choice of T_i, which affects also R_i. If, for example, PYTHIA QCD does not provide a realistic model of the true spectrum, that can bias U_i, unless R_i and T_i are simultaneously wrong in such a way that T_i/R_i remains equal to the (unknown) actual ratio T_i'/R_i' in Eq. 3. The use of bins quite wider than the amount of smearing makes it more likely that, even if T_i is not modeled correctly, the ratio T_i/R_i in each bin will be approximately correct. In [2] the bins are safely wider than jet p_T resolution, and their edges are driven by experimental constraints, such as trigger thresholds.

To assess the uncertainty from possible wrong modeling of T_i, the MC events used to determine C_i were re-weighted in multiple ways. Their re-weighting was determined by functions smooth in jet p_T, chosen so as to bracket the variation observed by varying parton density functions, by including next-to-leading-order corrections to QCD, as well as the difference observed between D_i and R_i. For each set of re-weighted MC events both T_i and R_i were re-computed, and so was C_i for each bin i. The largest variation observed in each C_i was taken as a systematic uncertainty.

2.3.4 Jet energy scale uncertainty

By far the dominant uncertainty in the final U_i comes from the uncertainty in jet energy scale (JES). All previous uncertainties, added in quadrature, amount to about 5% of relative uncertainty in C_i, which is the error band shown in Fig. 2. The rest $\sim$40% of uncertainty in the final answer comes from the JES uncertainty, and it dominates the blue error band in Fig. 1.

To propagate the JES uncertainty, the reconstructed p_T of all jets in MC events is shifted by ±1 standard deviation, the exact size of which is a function of jet p_T and pseudo-rapidity η. That affects R_i strongly, while T_i doesn't change, therefore C_i varies significantly. By applying on D_i the two alternative values of C_i, from the positive and the negative JES shift, two extreme U_i values are obtained for each bin i, whose distance is considered as the JES uncertainty on U_i.

3 Iterative unfolding

ATLAS used D' Agostini's iterative unfolding [1] in the study of minimum bias pp collisions [3]. The example to be shown is the estimation of the truth-level distribution of the multiplicity of charged particles. The result of this analysis is shown in Fig. 5.

3.1 Method description

The full method is clearly described in the original article [1] by D' Agostini. This paragraph will make a connection between the quantities in [3] and the notation used in [1].

Let n_{ch} be the number of charged particles produced in a pp collision. This is the truth-level quantity whose distribution needs to be estimated. It corresponds to the "cause" C mentioned in [1].

Let n_{trk} be the number of reconstructed tracks in a pp collision, which satisfy the selection criteria listed in [3]. It corresponds to the "effect" E mentioned in [1].

The reconstructed tracks are typically fewer than the actual charged particles, due to tracking inefficiency, therefore typically $n_{trk} \leq n_{ch}$. Therefore the migrations matrix is highly non-diagonal, and schematically looks like Fig. 6.

Re-writing the basic formulas from [1], substituting $C \rightarrow n_{ch}$ and $E \rightarrow n_{trk}$, we get

$$\hat{N}(n_{ch}) = \frac{1}{\epsilon(n_{ch})} \sum_{n_{trk} \geq 2} N(n_{trk}) P(n_{ch}|n_{trk}) \qquad \epsilon(n_{ch}) \neq 0, \qquad (7)$$

$$P(n_{ch}|n_{trk}) = \frac{P(n_{trk}|n_{ch}) P_0(n_{ch})}{\sum_{n_{ch} \geq 1} P(n_{trk}|n_{ch}) P_0(n_{ch})}, \qquad (8)$$
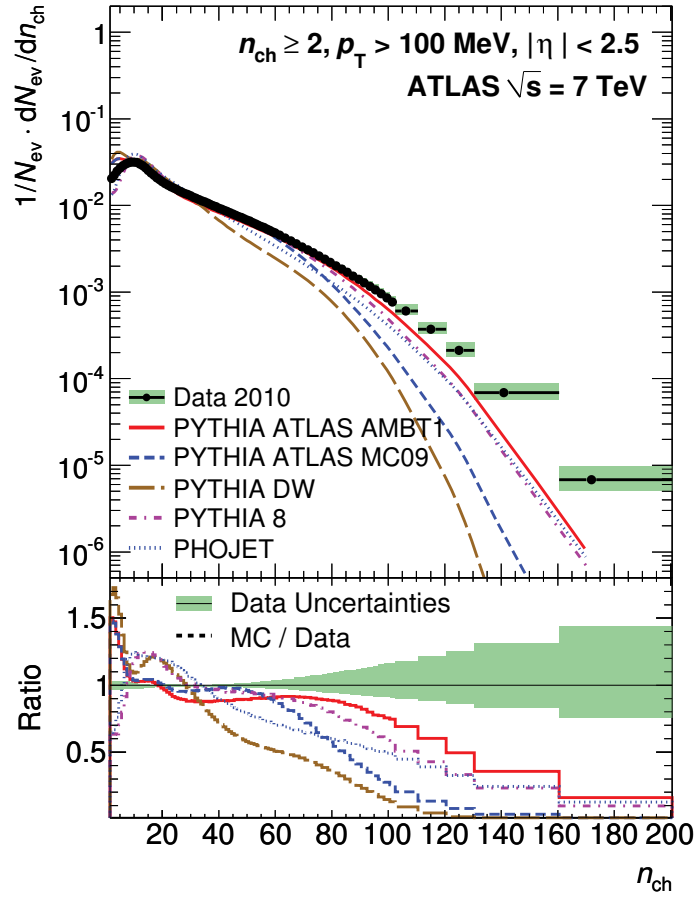
Fig. 5: The estimated spectrum of charged particle multiplicity (filled circles) in minimum bias pp interactions, from [3]. The statistical uncertainty is smaller than the marker size, and the asymmetric color band represents the total systematic uncertainty. Various theoretical predictions are overlaid for comparison.
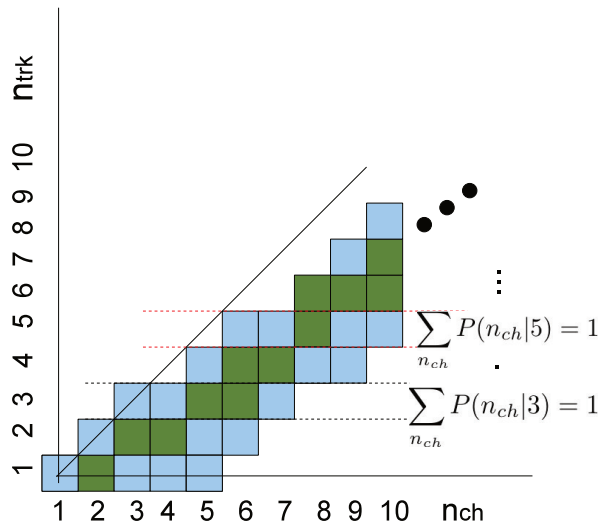
Fig. 6: Schematic representation of migrations matrix. The dark green squares represent higher probability than the light blue. Initially each matrix element equals the probability of MC events to contain n_{ch} charged particles and to have n_{trk} reconstructed tracks that satisfy the criteria listed in [3]. Then, the elements of each row, corresponding to a fixed n_{trk}, are normalized to have sum 1.

where the efficiency $\epsilon(n_{ch})$ corresponds to the probability of reconstructing at least two tracks, a requirement related to having a reliable primary vertex reconstruction, for a given number of charged particles:

$$\epsilon(n_{ch}) = P(n_{trk} \geq 2 | n_{ch}). \tag{9}$$

The term $P_0(n_{ch})$ is an arbitrary initial distribution for the truth-level quantity n_{ch}. The symbol $N(n_{trk})$ denotes the population of events where n_{trk} tracks were reconstructed, and $\hat{N}(n_{ch})$ is the estimator of the population of events with n_{ch} charged particles at truth-level.

3.1.1 Initial distribution and iterations

In [3], the initial distribution was defined to be the n_{ch} spectrum predicted by PYTHIA minimum bias MC. The reason is that the PYTHIA prediction has been tuned to data from various past experiments, so it is a reasonable starting point.

In iterative unfolding the number of iterations is decided arbitrarily. Too many iterations result in bin-by-bin fluctuations in the unfolded spectrum, similar to what one may get from simple migration matrix inversion [4]. Too few iterations increase too much the influence of the initial distribution on the final answer.

In [3], a convergence criterion was defined to determine when to stop iterating. The criterion was

$$\frac{\chi^2}{N_{bins}} < 1, \tag{10}$$

where

$$\chi^2 \equiv \sum_{i=1}^{N_{bins}} \left(\frac{n_{ch}^{i,current} - n_{ch}^{i,previous}}{\sqrt{n_{ch}^{i,previous}}} \right)^2. \tag{11}$$

Namely, iterations continued until the latest unfolded spectrum ($n_{ch}^{current}$) remained statistically consistent with the spectrum from the previous iteration ($n_{ch}^{previous}$). It was found that 4 iterations were enough to meet this convergence criterion.

3.1.2 The term $\epsilon(n_{ch})$

In principle one should extract $\epsilon(n_{ch})$ defined in Eq. 9, directly from the MC events used to populate the migrations matrix (Fig. 6). However, a decision was made in [3] to use instead a parametric approximation of $\epsilon(n_{ch})$.

Making the simplification that each charged particle has the same "average effective" probability ϵ_{eff} of being reconstructed as a track, the probability of having at least two reconstructed tracks is given by

$$f(n_{ch}) = 1 - (1 - \epsilon_{eff})^{n_{ch}} - n_{ch}(1 - \epsilon_{eff})^{(n_{ch}-1)}\epsilon_{eff}. \tag{12}$$

The unknown parameter ϵ_{eff} was adjusted so as make $f(2)$ equal to the $\epsilon(n_{ch} = 2)$ obtained from MC. The resulting value for ϵ_{eff} is within 4% from the average probability of track reconstruction that is determined from MC simulation, which indicates that $f(n_{ch})$ matches well the MC-driven $\epsilon(n_{ch})$ even for $n_{ch} > 2$.

After adjusting ϵ_{eff} as described, the quantity $f(n_{ch})$ from Eq. 12 substitutes $\epsilon(n_{ch})$ in Eq. 7. Practically this efficiency becomes $\simeq 1$ for $n_{ch} > 4$, and that is true regardless of using $f(n_{ch})$ or $\epsilon(n_{ch})$.

3.2 Statistical uncertainty

In Eq. 7, the estimator $\hat{N}(n_{ch})$ depends on the measured $N(n_{trk})$, which are the result of independent Poisson fluctuations. Simple error propagation would lead to the following standard deviation for $\hat{N}(n_{ch})$:

$$\sigma_{\hat{N}(n_{ch})} = \sqrt{\sum \left(\frac{1}{\epsilon(n_{ch})} P(n_{ch}|n_{trk}) \right)^2 N(n_{trk})}. \tag{13}$$

The way statistical uncertainty was actually calculated in [3] was

$$\sigma_{\hat{N}(n_{ch})} = \sqrt{\hat{N}(n_{ch})}. \tag{14}$$

Either way, the statistics in all bins of n_{trk} are high enough to make the statistical uncertainty negligible. In Fig. 5, the statistical error bars are invisible.

3.3 Systematic uncertainty

The following main sources of systematic uncertainty will be discussed:

i)   The choice of initial distribution $P_0(n_{ch})$;
ii) The uncertainty in track reconstruction efficiency;
iii) The uncertainty in MC spectrum.

3.3.1 Choice of initial distribution

The stability of the answer under different choices of initial distribution $P_0(n_{ch})$ was tested by assuming a "flat" initial distribution $P_0(n_{ch}) = 1$, and repeating the iterative unfolding procedure. This choice is obviously physically absurd; its purpose was only to show that even under extreme choices of $P_0(n_{ch})$ the answer $\hat{N}(n_{ch})$ doesn't change much.

Starting from a flat initial distribution, the number of iterations required to converge (Eq. 10) increased from 4 to 7. The final answer changed by less than 2% in all bins of n_{ch}, which was taken as a systematic uncertainty in $\hat{N}(n_{ch})$.

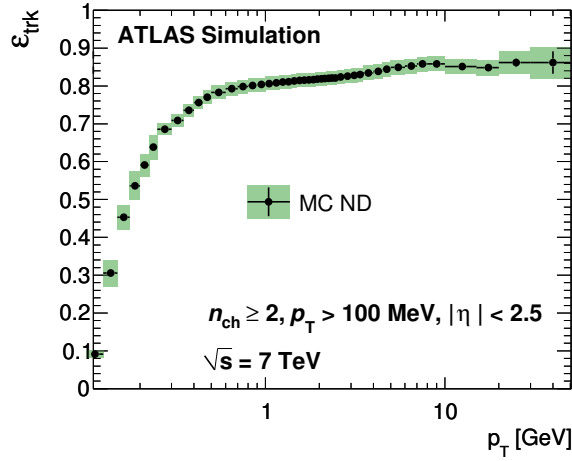### 3.3.2 Track reconstruction efficiency uncertainty

The main effect this unfolding is correcting is the inefficiency of tracking. This inefficiency is reflected in the probabilities of Eq. 7, and is obtained from MC simulation. If tracking inefficiency in MC is wrong, so is the obtained spectrum after unfolding.

Fig. 7 shows the track reconstruction efficiency (ϵ_{trk}) in ATLAS simulation.

To propagate the uncertainty of ϵ_{trk} into $\hat{N}(n_{ch})$, the natural thing to do would be to shift systematically ϵ_{trk}, thus changing $P(n_{ch}|n_{trk})$, and see how much $\hat{N}(n_{ch})$ would change. Instead, what was done in [3] was to keep the migration probabilities fixed, and modify the data ($N(ch_{trk})$) on which iterative unfolding was applied. The way in which the data were modified is described next.

Assume an event in data has n_{trk} tracks. Take one of these tracks. Its p_T corresponds to some efficiency ϵ_{trk} (Fig. 7). For the sake of clarity, let's say it corresponds to $\epsilon_{trk} = 0.80 \pm 0.05$. This ϵ_{trk} gets reduced by 1 standard deviation, so it is brought down to 0.75. For this reduced ϵ_{trk}, the expected number of tracks is $\frac{1}{0.80} \times 0.75 \simeq 0.94$. The track is then randomly kept, with probability 0.94, or discarded, with probability 0.06. This procedure of efficiency reduction and random removal is repeated for all n_{trk} tracks of the event. In the end, the event is left with n'_{trk}, where $n'_{trk} \leq n_{trk}$.

The above procedure is repeated for all data events, reducing n_{trk} to n'_{trk} in each event. Then, the distribution $N(n'_{trk})$ is unfolded instead of $N(n_{trk})$, which results in $\hat{N}'(n_{ch})$ instead of $\hat{N}(n_{ch})$.

Fig. 7: Track reconstruction efficiency ϵ_{trk} in ATLAS simulation. The error band represents its systematic uncertainty.

The above procedure could only remove tracks, not create any. However, the ϵ_{trk} uncertainty is symmetric, which means that the actual ϵ_{trk} could be also greater than its nominal value. For this reason, the difference between $\hat{N}(n_{ch})$ and $\hat{N}'(n_{ch})$ is symmetrized, and used as a systematic uncertainty in $\hat{N}(n_{ch})$. That means, for example, that if in a bin of n_{ch} the $\hat{N}'(n_{ch})$ was 5% greater than $\hat{N}(n_{ch})$, the uncertainty is set to $\pm 5\%$.

3.3.3 Uncertainty due to spectrum shape

The observed spectrum of track transverse momentum (p_T^{trk}) disagrees with the MC prediction after full ATLAS detector simulation, as shown in Fig. 8. This discrepancy is related to the unfolding from n_{trk} to n_{ch}, because ϵ_{trk} is a function of p_T^{trk} (Fig. 7). If the p_T^{trk} is not realistically modeled, neither is ϵ_{trk}.

The way this was treated was the following: In each bin of n_{trk}, the mean ϵ_{trk} was found by looping through all data events in the bin, and corresponding each observed p_T^{trk} to the value of ϵ_{trk} obtained from MC (Fig. 7). The same was then done for MC events in bins of n_{trk}, again corresponding the p_T^{trk} in MC events to values of ϵ_{trk} from Fig. 7. In each bin of n_{trk}, the average track reconstruction efficiency $\langle \epsilon_{trk} \rangle$ from data was compared to the same quantity from MC. The same $p_T^{trk} \rightarrow \epsilon_{trk}$ correspondence was used for both data and MC tracks, therefore the difference in the resulting $\langle \epsilon_{trk} \rangle$ is due to the different p_T^{trk} distributions.

In each bin of n_{trk}, if $\langle \epsilon_{trk} \rangle$ is larger in data than in MC, then the efficiency in data gets reduced by the observed difference, in the same stochastic way described in Section 3.3.2. This results in a different number of tracks $n'_{trk} \leq n_{trk}$ for each event in the data. The iterative unfolding is then applied to $N(n'_{trk})$, and a different estimator of the truth-level spectrum is obtained ($\hat{N}'(n_{ch})$). The difference between the nominal $\hat{N}(n_{ch})$ and $\hat{N}'(n_{ch})$ is found, and is used as a one-sided systematic uncertainty in $\hat{N}(n_{ch})$.

In n_{trk} bins where the $\langle \epsilon_{trk} \rangle$ in data is smaller than in MC, one would ideally wish to increase the ϵ_{trk} of the data, but it is not possible to create tracks, as explained in Section 3.3.2. Instead, the ϵ_{trk} of data is *reduced* by the observed difference, as if the data had greater $\langle \epsilon_{trk} \rangle$ than the MC. This results in a different data spectrum $N(n'_{trk})$, which after unfolding results in a different estimator $\hat{N}'(n_{ch})$. The difference between the nominal $\hat{N}(n_{ch})$ and $\hat{N}'(n_{ch})$ is found, and instead of using it directly as a one-sided systematic uncertainty in $\hat{N}(n_{ch})$, we use its opposite, to take into account the fact that the data ϵ_{trk} was reduced instead of increased.

The above procedure results in an asymmetric systematic uncertainty. The upper and lower uncer-
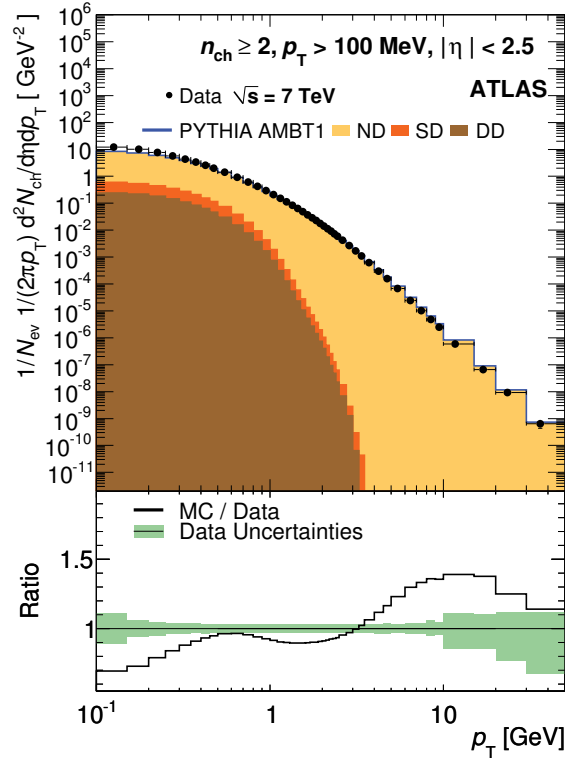
Fig. 8: The observed spectrum of p_T^{trk}, compared to the spectrum expected from MC simulation.

tainty are separately added in quadrature with the other systematic uncertainties, which are symmetric. This results in two unequal total systematic uncertainties, one suggesting that $N(n_{ch})$ could be above and the other below its nominal value. This asymmetric systematic uncertainty appears as a colored band in Fig. 5.

4 Concluding remarks

Two examples were shown of how unfolding has been used in ATLAS. They were chosen to be representative of different cases; one is using the bin-by-bin factors to correct the spectrum of a continuous observable (jet p_T), whereas the other uses iterative unfolding to estimate the truth-level distribution of a discrete variable (n_{ch}). The systematic uncertainties are quite different, as one analysis deals mainly with energy smearing, and the other with tracking inefficiency.

As of the time of this workshop, ATLAS has used extensively bin-by-bin correction factors, and in some cases iterative unfolding. More methods are being considered for future iterations of some of these analyses.

Unfolding has been used only in analyses where the goal was to estimate a truth-level distribution. Unfolding has been deliberately avoided in searches for new physics, where bias in bins with low statistics can not be afforded, where it can not be assumed that the data are consistent with the MC prediction as is silently assumed in some stages of unfolding, and where Poisson-distributed data are simpler to evaluate than estimators resulting from unfolding procedures after a series of arbitrary regularization choices. There are several unfolding methods, in some of which anomalies due to new physics could even be reduced, whereas the observed data are unique. Any inference is possible using directly the data, without unfolding, and a theoretical prediction that either includes full detector simulation, or at least an approximation of it that amounts to the inverse of unfolding, namely folding, which can be done with no need for regularization. The only task for which unfolding is strictly needed is the estimation of a truth-

level spectrum, whose later use to make statistical inferences becomes complicated by non-Poissonian statistics, biases that are hard to estimate, and bin-to-bin correlations.

In none of the analyses where unfolding was used was the full covariance matrix provided. The latter would be necessary to correctly compare a truth-level theoretical prediction to the result of unfolding. In most cases the comparison between the result of unfolding and the truth-level Standard Model prediction is made qualitatively, avoiding to provide a p-value that would require proper use of the covariances between bins. When a more quantitative comparison is attempted, like in [6], a χ^2 is used only as a metric to determine if one theory agrees with the data more than another, but not as a test statistic to compute a p-value.

Acknowledgements

References

[1] G. D' Agostini, *A Multidimensional Unfolding Method Based On Bayes' Theorem* Nucl. Instr. and Meth. in Phys. Res. A362 (1995) 487

[2] ATLAS Collaboration, *Measurement of inclusive jet and dijet cross sections in proton-proton collisions at 7 TeV centre-of-mass energy with the ATLAS detector*, Eur.Phys.J.C71:1512,2011, arXiv:1009.5908v2 [hep-ex]

[3] ATLAS Collaboration, *Charged-particle multiplicities in pp interactions measured with the ATLAS detector at the LHC*, arXiv:1012.5104, accepted by New Journal of Physics.

[4] Glen Cowan, *A Survey Of Unfolding Methods For Particle Physics*, available at the URL `http://www.ippp.dur.ac.uk/old/Workshops/02/statistics/proceedings/cowan.pdf`

[5] ATLAS Collaboration, *Measurement of the inclusive isolated prompt photon cross section in pp collisions at $\sqrt{s}$ = 7 TeV with the ATLAS detector*, arXiv:1012.4389v2 [hep-ex], submitted to Phys. Rev. D.

[6] ATLAS Collaboration, *Study of Jet Shapes in Inclusive Jet Production in pp Collisions at $\sqrt{s}$ = 7 TeV using the ATLAS Detector*, arXiv:1101.0070v1 [hep-ex], submitted to Phys. Rev. D.

[7] ATLAS Collaboration, *Measurement of the production cross section for W-bosons in association with jets in pp collisions at $\sqrt{s}$ = 7 TeV with the ATLAS detector*, arXiv:1012.5382v2 [hep-ex], submitted to Physics Letters B.

[8] T. Sjostrand, S. Mrenna and P. Z. Skands, JHEP **0605**, 026 (2006) [arXiv:hep-ph/0603175].

[9] ATLAS Collaboration, *Properties of Jets and Inputs to Jet Reconstruction and Calibration with the ATLAS Detector Using Proton-Proton Collisions at $\sqrt{s}$=7 TeV*, ATLAS-CONF-2010-053, available at the URL `http://cdsweb.cern.ch/record/1281310`

[10] ATLAS Collaboration, *Jet energy resolution and selection efficiency relative to track jets from in-situ techniques with the ATLAS Detector Using Proton-Proton Collisions at a Center of Mass Energy $\sqrt{s}$ = 7 TeV*, ATLAS-CONF-2010-054, available at the URL `http://cdsweb.cern.ch/record/1281311`